Chin. J. Astron. Astrophys. Vol. 0, No. 0, (200x) 000–000
(*http://www.chjaa.org*)

Chinese Journal of Astronomy and Astrophysics

General Relativistic Radiative Transfer: Applications to Black-Hole Systems

Kinwah Wu[1]*, Steven V. Fuerst[2], Yosuke Mizuno[3], Ken-Ichi Nishikawa[3], Graziella Branduardi-Raymont[1] and Khee-Gan Lee[1,4]

[1] Mullard Space Science Laboratory, University College London, Holmbury St Mary, Surrey RH5 6NT, United Kingdom
[2] Kavli Institute for Particle Astrophysics and Cosmology, Stanford University, Stanford, CA 94304, USA
[3] NASA-MSFC/NSSTC, 320 Sparkman Drive, Huntsville, AL 35805, USA
[4] Department of Astrophysical Sciences, Princeton University, Princeton, NJ 08544, USA

Received 2007 month day; accepted 2007 month day

Abstract We present general relativistic radiation transfer formulations which include opacity effects due to absorption, emission and scattering explicitly. We consider a moment expansions for the transfer in the presence of scattering. The formulation is applied to calculation emissions from accretion and outflows in black-hole systems. Cases with thin accretion disks and accretion tori are considered. Effects, such as emission anisotropy, non-stationary flows and geometrical self-occultation are investigated. Polarisation transfer in curved space-time is discussed qualitatively.

Key words: accretion, accretion disks – black hole physics – galaxies:active — radiative transfer — relativity

1 INTRODUCTION

Observations of the AGN MCG-6-30-15 by *ASCA* showed Fe Kα emission line with a very broad asymmetric profile (Tanaka et al. 1995). The presence of the line was confirmed by later observations using e.g. *Chandra* and *XMM-Newton*. The broad asymmetric Fe Kα lines have also been seen in the spectra of several other AGN (e.g. NGC3516, Nandra et al. 1999). The line is believed to be fluorescent emission from accretion flows very close to the black-hole event horizon, where gravitational and kinematic effects are important. There are several mechanisms contributing to the line broadening and profile modification. The rotational motion in the accretion disk causes the two peaks of the line; relativistic boosting makes the line asymmetric (with an enhanced blue (high-energy) line peak and a suppressed red (low-energy) peak); time dilation, due to gravity and transverse relativistic motion, broadens the line and shifts it to a

* E-mail: kw@mssl.ucl.ac.uk (kw), sfuerst@stanford.edu (svf)

lower energy. (See e.g. review by Fabian et al. 2000.) Gravitational lensing also alters the line profile by affect the projection of the emission.

Modeling relativistic lines from black-hole system have been carried out since the 70's. In spite of the variations in the numerical/analytic techniques, line-profile calculations generally follow a prescription which can be summarised as follow. (1) Define the space-time metric. (2) Construct a model flat accretion disk to give a macroscopic velocity profile for the emitters. The disk can be stationary or time-dependent, Keplerian or non-Keplerian. Usually a parametric emissivity profile is assumed. Local variations in the disk emission are modeled through parametric prescriptions of turbulence, or density/emissivity inhomogeneities, time-dependent flares ..... etc. (3) Determine the geodesics of the "observable" photons and calculate the relative energy shifts of the photons between the emitter and the observer. (4) Bin the photons according to their energies and sum the bins to produce the line spectrum. For time-dependent line profile calculations, the photons are also time binned and summed, according to their arrival time. These calculations have provided insights for our understanding of relativistic effects on line profile in accreting black holes. However, as our observational capability improves, we need more sophisticate radiative transfer calculations for emission from black-hole systems in order to fully utilise the high quality spectral and timing data that will be collected by the next generation observatories.

2 RADIATIVE TRANSFER FORMULATION

Unless otherwise stated, we use the convention of natural unit ($c = G = \hbar = 1$, where c is the speed of light, G is the gravitational constant, and $\hbar$ is the Planck constant). Without scattering, the general relativistic transfer equation reads

$$\frac{d\mathcal{I}}{d\lambda} = k_\alpha \frac{\partial \mathcal{I}}{\partial x^\alpha} - \Gamma^\alpha_{\beta\gamma} k^\beta k^\gamma \frac{\partial \mathcal{I}}{\partial k^\alpha} = k_\alpha u^\alpha|_\lambda \left[-\chi_o(x^\beta,\nu)\mathcal{I} + \eta_o(x^\beta,\nu)\right] \quad (1)$$

(Baschek et al. 1997; Fuerst & Wu 2004; Wu et al. 2006, see also Lindquist 1996), where λ is the affine parameter, $\Gamma^\alpha_{\beta\gamma}$ is the affine connection (determined by the metric $g_{\alpha\beta}$, which is specified by $d\tau^2 = g_{\alpha\beta}dx^\alpha dx^\beta$), k^α is the 4-momentum of photons, and u^α is the 4-velocity of the medium. The Lorentz invariant intensity $\mathcal{I} \equiv I_\nu/\nu^3$, where I_ν is the specific intensity, ν is the frequency, and χ_o and η_o are the Lorentz invariant absorption and emission coefficients respectively. (The subscript "o" denotes that the variable is evaluated at the local rest frame.) This formulation allows the radiation to be self-absorbed internally in the emitting medium, and absorption and re-emission in external line-of-sight media. Once the photon geodesics are determined and the emission and absorption coefficients are given, the radiative-transfer equation can be solved along the line-of-sight (Fuerst & Wu 2004) using a ray-tracing, and the spectrum of the emission is determined.

In the presence of scattering, photons are injected into the line-of-sight from a crossing ray. Equation (1) is therefore inadequate. In principle, adiative transfer in a scattering medium must be evaluated globally, instead of tracing individual rays independently each time. Obtaining a solution to the equation is, however, not straightforward and often practically impossible. Various techniques have been developed to bypass a direct evaluation of the proper integro-differential radiative transfer equation, for example, to obtain a solution to a set of differential equations, that approximate the exact radiative transfer equation.

For general relativistic radiative transfer for emission from accreting black holes in AGN, the moment methods described in Fuerst (2005) is generally applicable. The method may be summarised as follow. First, expand the intensity $\mathcal{I}(x^\alpha, k^\alpha)$ into a series using a set of orthogonal

symmetric tensors $J_{\alpha_1....\alpha_j}$, which gives

$$\mathcal{I}(x^\alpha, k^\alpha) \;=\; a_0 J + \sum_{i=1}^{\infty} a_i J_{\alpha_1\alpha_2....\alpha_i} n^{\alpha_1} n^{\alpha_2} ....n^{\alpha_i} \;, \tag{2}$$

where n^α is the directional unit vector of the photon. Next, generate a set of projected tensors $\mathcal{J}_{\alpha_1\alpha_2....\alpha_i....}$ satisfying the condition:

$$u^\alpha \mathcal{J}_{\alpha\alpha_1\alpha_2....\alpha_i....} \propto \mathcal{J}_{\alpha_1\alpha_2....\alpha_i....} \;. \tag{3}$$

The 4-velocity u^α is specified in a preferred reference frame, such as the local rest-frame of the medium. We then consider an approximation by truncating the moment expansion. For the j-th order, we have

$$\mathcal{I}_j(x^\alpha, k^\alpha) \;=\; \mathcal{J}_{\alpha_1\alpha_2....\alpha_j} m^{\alpha_1} m^{\alpha_2} ....m^{\alpha_j} \;, \tag{4}$$

where $m^\alpha = n^\alpha + u^\alpha$. With these, we derive moment equations, whose of solutions $\mathcal{J}_{\alpha_1\alpha_2....\alpha_i}$ form the basis for the construction of various order approximations to the 'true' intensity $\mathcal{I}(x^\alpha, k^\alpha)$.

For instance, if opacity of the medium is contributed by three processes: a free-free process due to a sub-population of thermal electrons (of weight X), synchrotron radiation due to another sub-population of electrons which is non-thermal (of weight $(1-X)$), and electron scattering, the first-order moment equation will read

$$\begin{aligned} & m_\alpha \left[\mathcal{J}^\alpha{}_{,\beta} n^\beta + \Gamma^\alpha_{\beta\gamma} \mathcal{J}^\gamma m^\beta + \xi \left(\mathcal{J}^\alpha - \frac{\partial \mathcal{J}^\alpha}{\partial(\ln E)} \right) \right] \\ & \quad = \; -\left[X\sigma_{\rm ff} + (1-X)\sigma_{\rm syn} + \sigma_{\rm T} \right] \rho \mathcal{J}^\alpha m_\alpha + X\sigma_{\rm ff}\rho\mathcal{B} + (1-X)\sigma_{\rm syn}\rho\mathcal{S}_{\rm syn} + \sigma_{\rm T}\rho\mathcal{J}^\alpha u_\alpha \;, \end{aligned} \tag{5}$$

where $\sigma_{\rm ff,syn,T}$ are the respective absorption cross section of the free-free, synchrotron and electron scattering processes, $\mathcal{B} \equiv B_\nu/\nu^3$ is the Lorentz invariant Planck function, $\mathcal{S}_{\rm syn}$ is the corresponding Lorentz invariant source function for synchrotron radiation, and the variable

$$\xi \;=\; -\frac{1}{E^2}\frac{DE}{d\lambda} \;=\; u^\alpha n_{\alpha;\beta} n^\beta + n^\alpha u_{\alpha;\beta} u^\beta \tag{6}$$

(with $E \equiv \nu$ for the photons). If the synchrotron emission is from a thermal population of electrons, the source function $\mathcal{S}$ is the same as the Planck function $\mathcal{B}$. The equation is analogous to the conventional radiative transfer equation. The first group of terms on the right side correspond to removable of photons by various processes; the next term corresponds to free-free emission; the term after it corresponds to synchrotron emission; the last term corresponds to injection of photons into the line-of-sight via scattering. The second-order and higher-order equations can be derived accordingly, following similar procedures (Fuerst 2005).

3 THIN RELATIVISTIC ACCRETION DISKS

The radiative transfer formulations presented in §2 is applicable to a wide range of astrophysical settings. For emission lines from accretion and outflows in black-hole systems. both formulations easily generate relativistic lines as those in Cunningham (1975), Fabian et. al. (1989), Stella (1990), Laor (1991), ... by setting the absorption, emission and scattering coefficient to zero. The inclusion of absorption, emission and scattering coefficients, the formulations take account of the full transfer effects.

We show in the following subsection two examples of applications for geometrically thin relativistic accretion disks around black holes. The first one concerns angle-dependent effects

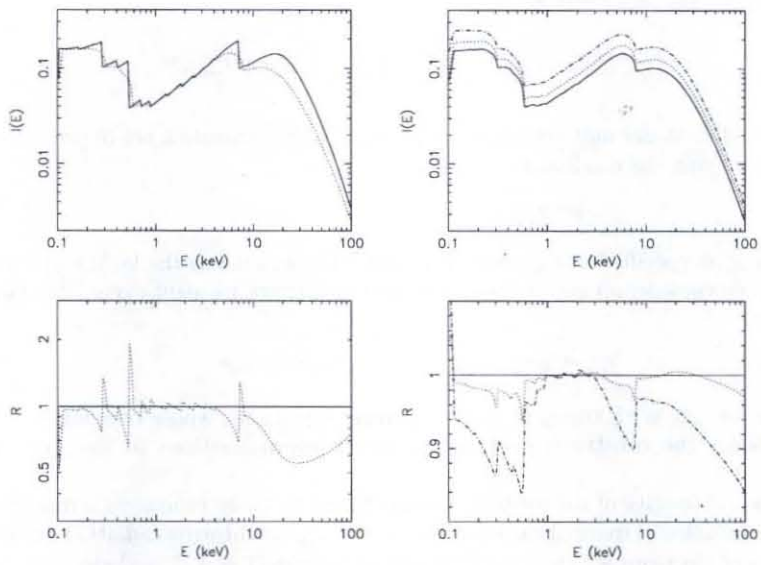

Fig. 1 The top panel of the left column shows the comparison between a reflection spectrum of a geometrically thin relativistic accretion disk around a Schwarzschild black hole (dotted line) and a rest-frame reflection spectrum (solid line) generated by PEXRAV in XSPEC based on the model calculation of Magdziarz & Zdziarski (1995). The viewing inclination angle of the disk is 45°. The strength of the reflection follows a radial power-law profile with an index of −2. The bottom panel of the column shows the corresponding quotient spectra, which is obtained by dividing the spectra by the rest-frame spectrum. The top panel of the right column show reflection spectra of thin accretion disks around black holes with spin parameters $a = 0$, 0.5 and 0.998 (solid, dotted and dot-dashed lines respectively). The bottom panel of the column shows the corresponding quotient spectra, in reference to the case with $a = 0$. In all the reflection spectra the intensity $I(E)$ is in an arbitrary unit. The quotient spectra are normalised, with the normalised intensity $R = 1$ at the energy $E = 1$ keV.

on the reflection continuum. The second concerns a complex situation that the emitting and absorbing media vary with time and that emission and absorption are not confined to the disk equatorial plane, so that angle-dependent effects are treated explicitly throughout the entire region.

3.1 angle-dependent emission - reflection spectra

An AGN X-ray spectrum generally consists of a thermal black-body component, a hard power-law component, a reflection component, and lines, e.g. the fluorescent Fe Kα line. The thermal black-body component, the power-law component and the lines are probably isotropic. The reflection component is, however, strongly viewing angle dependent. In the analyses of X-ray spectra data, model fits to the reflection component often assume a fix viewing angle, chosen to be the same as the viewing inclination of the normal of a geometrically thin accretion disk. This assumption can be problematic, as the space-time in the inner accretion disks is curved

and the emission is gravitational lensing. The pitch angles of the photons from a disk surface element that reach a distant observer are not the same as the inclination angle specifying the orientation of the accretion disk. Light aberration is also non-negligible as the flows in the inner accretion disk are highly relativistic. The situation is further complicated by the rotation of the black hole, which leads to reference frame dragging. Moreover, limb effects occurs when the emission emerging from the disk surface. (See Lee et al. (2007) and Wu et al. (2006).)

Gravitational and relativistic kinematic effects coupling with angle-dependence of reflection will lead to a number of observable consequences. Figure 1 illustrated some of the consequences by (i) a comparison between a relativistic disk reflection spectrum and a rest-frame spectrum, and (ii) a comparison between reflection spectra from accretion disks around black holes with different spin parameters. The first demonstrates how local angle-dependence together with relativistic energy shift modifying the reflection continuum. The second shows how the effects combine with the rotation of the black hole, giving rise to broad features mimicking relativistic emission lines.

An obvious difference between a relativistic reflection spectrum and a rest-frame spectrum is the smearing of the absorption edges. The quotient spectra in Fig. 1 imply that fitting data of a reflection spectrum of a relativistic accretion disk using a model rest-frame reflection spectra will result in flux excess blue-ward of the edge and flux deficiency red-ward of the edge. These may lead to an artifact blue-shift emission line, which has a wavelength consistent with the element species associated with the edge. The artifact feature may also be mistaken as an emission line from relativistic outflows. Another obvious difference is at the $10 - 100$ keV spectral region. The reflection peak is lowered and the high-energy tail is flattened in the relativistic spectrum. These will affect the slope of the fit power-law for the observed spectrum. The effect is severe in situations where the spectral coverage at the high-energies, say above 20 keV, is unavailable.

The effects of the black hole's rotation on the reflection spectra of relativistic disks are manifested predominantly in the red-ward region of the absorption edge (panels in the right column. Fig. 1. The disk reflection spectrum of a fast rotating black hole shows flux deficiency red-ward of the edge when comparing with the disk reflection spectrum of a slower rotating black hole. Using spectral models corresponding to fast rotating black hole in fits to the spectra data of a system with a slowly rotating black hole will therefore yield flux excess red-ward of the edge. The flux excess may create a line-like feature with a profile resembling those of relativistic emission lines for Schwarzschild black hole or even fast rotating Kerr black holes, depending the relative rotational rate of the two black holes in the comparison. The high-energy tail of the reflect spectrum is also affected by the black-hole spin. The general trend is that he more rapidly is the rotation of the black hole the steeper the slope of the high-energy spectral tail.

3.2 time-varying accretion and outflow

The current time-dependent calculations of emission from relativistic flows are mostly focused on effects of dynamics. They generally employ a generic ray-tracing algorithm which does not include opacity effects in the emitting and transmitting media. Although these studies have provided great insights on how space-time curvature and relativistic kinematics on X-ray spectral formation in accreting black holes, for proper calculations of emission from magnetised disk-outflow system, one needs to take full account of radiative transfer to treat the emission and absorption processes explicitly.

The change of an emission spectrum with the viewing inclination of a system is not restricted to photon pitch-angle isotropy in reference to the normals of the emission surface elements. It also occurs when the emission or absorption of the line-of-sight material is anisotropic. For

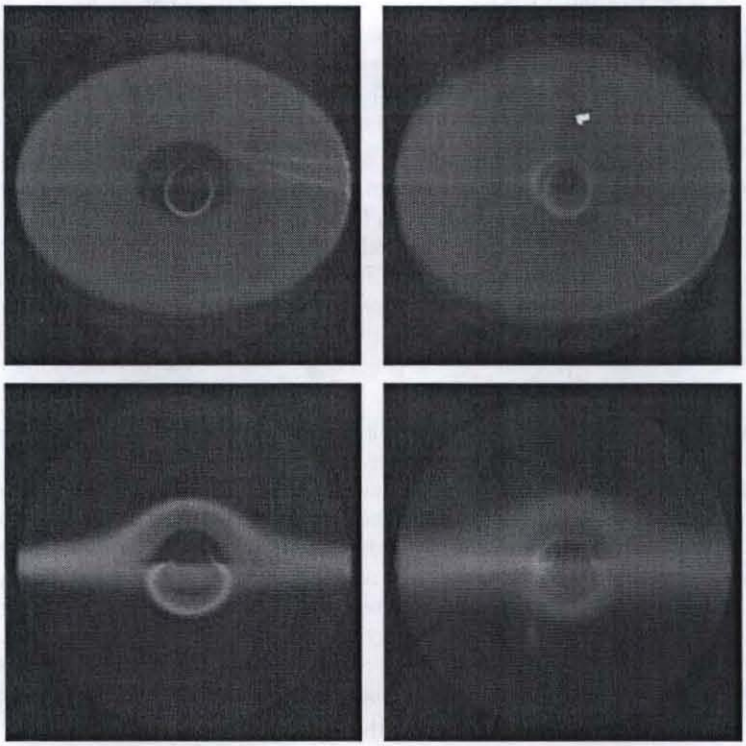

Fig. 2 The panels on the top row show images of emissions from the flows, viewed at an inclination angle of 45°, at time $t/\tau_s = 0$ (left) and 300 (right) (where $\tau_s = r_s/c$, with r_s is the Schwarzschild radius of the black hole), corresponding to an initial state and a later state of the simulation. Bright synchrotron filaments (in greenish blue colour) are seen near the disk surface. The bright blue ring at the center is first-order lensed disk image. The fuzzy yellowish ring near the center in the image at $t/\tau_s = 300$ is due to direct thermal free-free emission from dense material piled up in the inner accretion disk. The panels on the bottom row show images of emissions from flows viewed at an inclination angle of 85° for $t/\tau_s = 0$ (left) and 300 (right). The faint vertical features below the disk are the components of the counterpart jet.

instance, synchrotron radiation is strongly beamed intrinsically, usually in the direction along the magnetic field line.

Magnetised accretion disks and outflows are known to be non-steady. The magnetic fields threading the flows are twisted continually and the local field strengths fluctuating. The rapid variations in the field configuration and in the flow coupling with the gravitational lensing give rise to a number of unexpected phenomena. Figure 2 shows emission from from a flat accretion disk and its outflow. The dynamical variables are obtained by 2.5-D general relativistic MHD simulations using the 3-D RAISHIN code (Mizuno et al. 2006a,b). In the radiative transfer calculations the opacity is assumed to be due to thermal free-free and synchrotron processes. Bright filaments are seen in the disk image. They are caused by chance alignment of magnetic

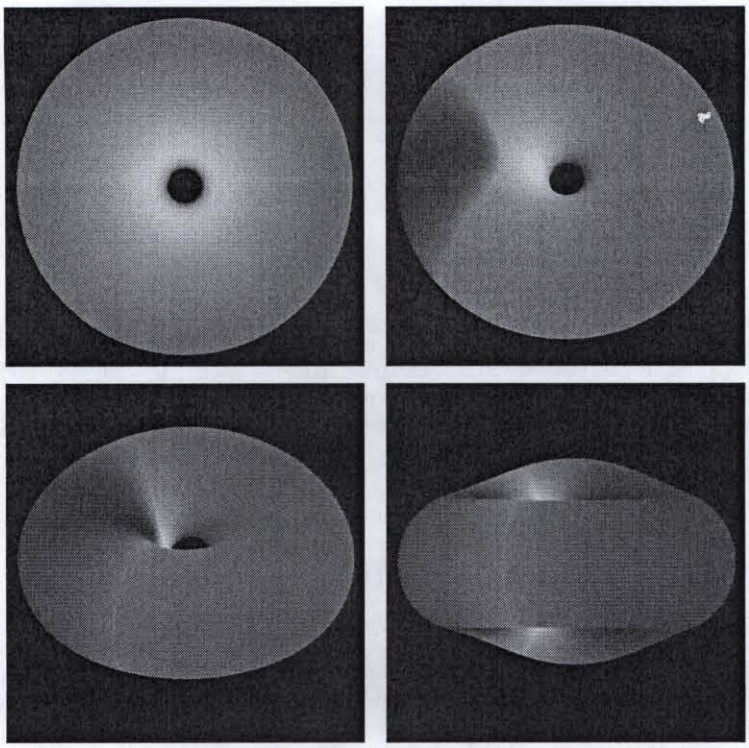

Fig. 3 Energy shift images of opaque relativistic accretion tori around a rotating black hole with a spin parameter $a = 0.998$, viewing at inclination angles $i = 1°$, $30°$, $60°$ and $89°$ (panels ordered from left to right and top to bottom). Red for red shifts in energy and blue for blue shifts. The tori have a rotational velocity profile index $n = 0.1$ (see Fuerst & Wu 2007) and the innermost boundary of the emission surface reaches $1.3r_{\rm g}$, where the gravitation radius $r_{\rm g} = 1$ for normalised black-hole mass.

field lines, along which synchrotron emission is beamed and hence boosted. As the simulations evolve, the filaments wiggle quasi-periodically (i.e. QPOs) on time scales of the order that of the dynamics of local flows. The filament features are robust — seen at all viewing inclinations. They are geometrical in nature, and are not sheared by the differential rotation of the accretion disk, This is in contrast to material clumps circulating around in the accretion disk, which disperse after a few orbits. Note that there is a pair of jets, with the counter-jet below the equatorial plane is visible. The simulations show two concentric components in each jet, each of which have different dynamical and emission properties, and a material piled up in the inner disk, giving rise to strong free-free emission.

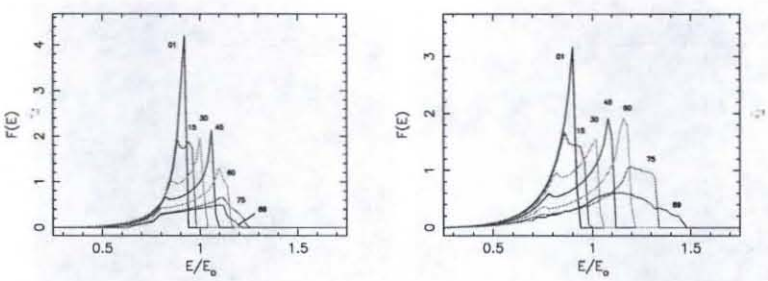

Fig. 4 The left panel shows the emission line profiles of an opaque torus with parameters as those in Fig. 3 (i.e. $n = 0.100$), viewed at inclination angles of $i = 1°$, $15°$, $30°$, $45°$, $60°$, $75°$ and $89°$. The right panel shows the emission line profiles of an opaque torus with parameters the same as those of the torus in the left panel except that $n = 0.001$ (i.e. practically a thin disk). The intensity $I(E)$ is normalised such that $I(E) = 1$ at $E/E_o = 1$ for $i = 45°$.

4 RELATIVISTIC ACCRETION TORI

4.1 Opaque tori

An accretion torus is a 3-D object, unlike a geometrically thin accretion disk, which is 2-D. Several methods commonly used in relativistic line calculations for thin accretion disks around black holes (e.g. Cunningham 1975) are not applicable, as for tori the emission originates from emission surfaces not in the equatorial plane. The situation is further complicated if the emission is angle dependent. While the entire upper surface of a geometrical thin accretion disk is always visible, self-occulation effects in tori are important at high viewing inclination angles (Fig. 3). This plays a very significant role in shaping the emission line profiles. Figure 4 shows the profiles of emission lines from two accretion tori with different thickness (specified by the velocity profile parameter, n, Fuerst & Wu 2007) viewing at various inclination angles. The torus with $n = 0.1$ has substantial thickness (see Fig. 3); the torus with $n = 0.001$ is practically the same as a geometrically thin disk. Both tori show similar line profiles at low inclination angles . The lines are red-shifted because of gravitational red-shift and transverse Doppler effect. The difference between lines from the two tori become more visible for viewing inclinations i larger than $\sim 45°$. At high inclination angles, the lines from tori with the larger n are narrower, i.e. suffer less red-shuft and less blue shift, as the innermost region, where relativistic effects are more severe, is not self-obscured. Here, it demonstrates that extracting information of the parameter of the system is non-trivial, as geometrical factors (such as aspect ratio of the accretion torus/disk) could affect maximum red-shift and maximum blue-shift in the line profile, thus causing confusing in the estimation of the location large stable particle orbit and hence the spin of the black hole.

4.2 Semi-transparent tori

Another different between an accretion torus and an accretion disk is that the emission is not restricted to a surface when the torus is not optically thin. In this situation, the emission seen by the distant observer is contributed by the entire accretion torus, as shown in Figure. 5). The relativistic beaming is more important than for that in opaque tori, where the most beamed/boosted emission is hidden because of self-occulation. If the torus is semi-opaque,

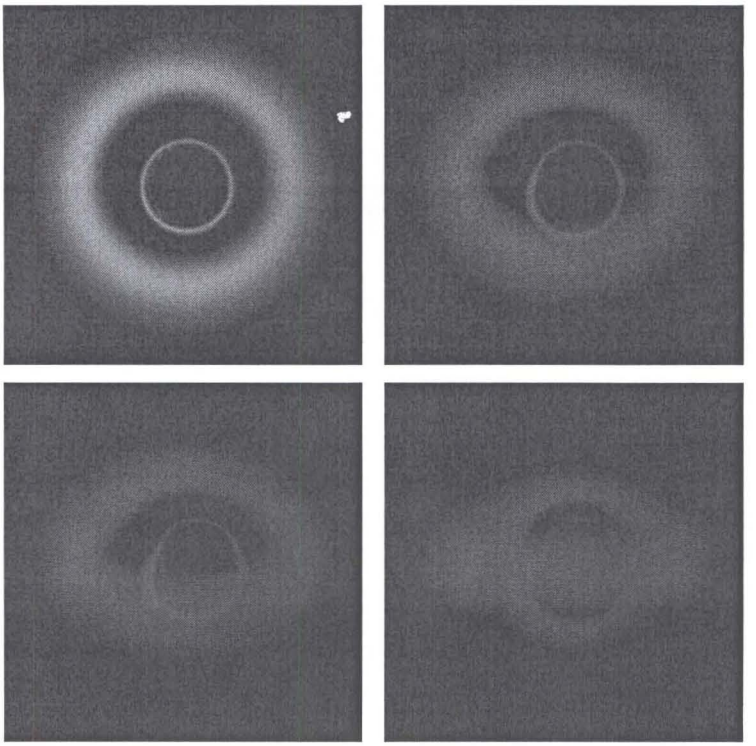

Fig. 5 Surface brightness of semi-transparent accretion tori around black holes with $a = 0.998$, viewed at inclinations $i = 15°, 45°, 60°$ and $85°$ (panels from left to right amd from top to bottom). The opacity is provided by the Fe Kα and Kβ lines. The brightness is normalised such that the maximum pixel brightnesses of all tori in the images are the same.

various complicated opacity effects may arise. For example, two lines with small difference in wavelengths, the line emitted from one part of the torus may be resonant with another line at the other part of the torus, because of the energy shifts during to velocity shears and difference in the gravitational potential of the emitters and the line-of-sight absorber/scatterer. While the emission lines from such tori are still broad and asymmetric as those of the opaque disks and torus, the line profiles are not at identical (Fuerst 2005).

4.3 Scattering dominated tori

In the scattering torus, the opacity is provided by electron scattering as well as the line/continuum emission and absorption processes. As photons can be scattered into a ray from a cross ray, the radiative transfer needs to be evaluated globally. With the moment formulation described in §2, the emission from scattering accretion tori can be calculated, and Figure 6 shows an example. Although a scattering torus may resemble a semi-transparent absorptive torus, the emission properties are very different. Firstly, line resonance is difficult to

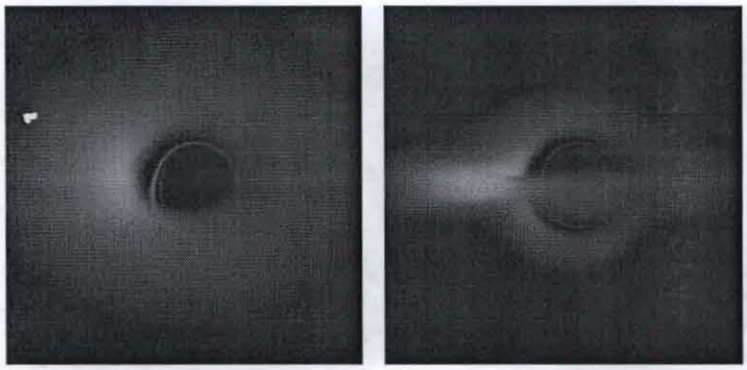

Fig. 6 Surface brightness of scattering accretion tori around black holes with $a = 0.998$, viewed at inclinations $i = 45^\circ$ (left) and 85° (right). The opacity is due to eleectron scattering. The brightness is normalised such that the maximum pixel brightnesses of the two tori are the same.

occur for a strongly scattering torus. Secondly, the beaming effects less obvious in a torus with electron scattering, as the beamed emission can be scattered out from the line-of-sight. This is in big contrast to to an absorptive torus, where a beamed line photon is highly energy-shifted that it will not suffer being resonant scattered/absorbed. The total emission from an opaque torus is the sum of weighted and shifted Planck function from the visible torus surface element. This is not true for a thick torus, the emission from a scattering thick torus is not necessarily thermal and the total emission from it is not simply summing the weighted and shifted local Planck function of the visible elements of the last scattering torus surface. In addition to all these, an opaque absorptive torus would not show strong polarisation, but a scattering thick torus is expected to be polarised.

5 BRIEF COMMENTS ON POLARISATION RADIATIVE TRANSFER

In Newtonian space-time, the polarised radiative transfer equation may be expressed as

$$\hat{\mathcal{D}}\, I_{\rm i}(\nu,\hat{\Omega}) \;=\; -K_{\rm ij} I_{\rm j}(\nu,\hat{\Omega}) + j_{\rm i}(\nu,\hat{\Omega}) + \int d\nu' \int d\hat{\Omega}'\; S_{\rm ij}(\nu,\nu';\hat{\Omega},\hat{\Omega}') I_{\rm j}(\nu',\hat{\Omega}')\;, \qquad (7)$$

where i and j are indices for the polarisation modes, $I_{\rm i}$ is the intensity of a polarisation mode, $j_{\rm i}$ is the emission coefficient, $K_{\rm ij}$ is the opacity whose diagonal elements specify absorption of the polarisation and off-diagonal elements specific polarisation conversion and rotation, $S_{\rm ij}$ is the scattering matrix, ν is the frequency of the radiation, and $\hat{\Omega}$ is the directional unit vector of the radiation propagation. The propagation differential operator is given by

$$\hat{\mathcal{D}} \equiv \frac{1}{c}\frac{\partial}{\partial t} + \hat{\Omega}\cdot\nabla\;. \qquad (8)$$

Equation (7) implies that the creation of a polariation mode and the conversion between different polarisation modes are caused by the meida, either the emitters or the line-of-sight material. For instance, in the presence of a magnetic field, gyrating electrons will give rise to cyclotron and

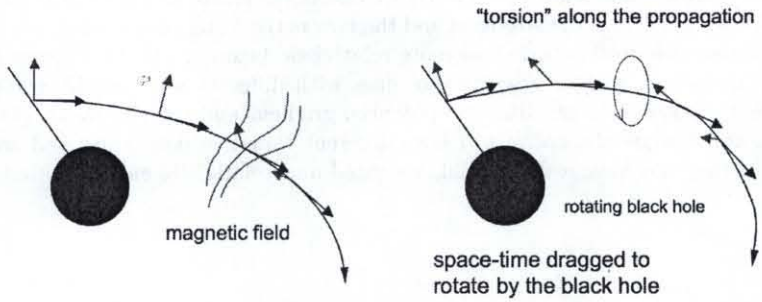

Fig. 7 Schematic illustrations showing the rotation of polarisation vectors in the presence of magnetic field (left) and in rotational space-time (right) as the radiation propagates.

synchrotron radiations, which are polarised. Also, the polarisation will undergo Faraday rotation/conversion when the radiations propagate in the magnetised plasma (see Fig. 7). Scattering processes may also induce polarisation. The propagation operator, however, does not affect the polarisation properties of the radiation. In curved space-time, this may not be true. 3-vectors defined on a local Lorentzian space-time are not preserved undergoing parallel transport along a geodesic (see e.g. Misner, Thorne & Wheeler 1973). As the radiation propagates in a curved space-time, the orientations and strengths of the electric and magnetic fields change as seen by a distant observer, resulting in rotation, stretching and twisting of the polarisation vectors. If the space-time is rotating, such as that around a Kerr black hole, the polarisation vector can also be dragged into rotation (Fig. 7). For radiative transfer in black-hole environments, conversion and rotation of the polarisation vector are caused by space-time curvature and rotation as well as the radiative properties of the emitters and the media through which the radiation propagates. To disentangle all these effects are non-trivial. However, before this difficult task is carried out, one needs a fully covariant polarisation radiative transfer formulation applicable and suitable for astrophysical settings, which is currently lacking.

6 SUMMARY

We present a general relativistic formulations for radiative transfer which treats emission and absorption processes explicitly. We also present a more general formulation which includes scattering in addition to emission and absorption. A moment solution is derived for this equation. The formulations are applicable for the calculations of emission from accretion disks and accretion tori around black holes. Cases of reflective flat disks, opaque tori, semi-transparent tori and scattering tori are presented to illustrate various effects, which have been failed to recognise by conventional ray-tracing relativistic line calculations. Polarisation transfer in curved space-time is briefly discussed.

We summary our findings as follow. (1) Angle-dependent effects are important and improper modeling of the reflection continuum will give rise to artifact features with profiles very similar to those of relativistic lines from accretion disks around fast rotating black holes. (2) Time dependent flows in the presence of magnetic fields together with relativistic beaming can give rise to QPOs in the emission. (3) Self-occulation is important for opaque accretion disks

with substantial thickness (i.e. accretion tori) at high viewing inclination angles. Lines from the thicker tori are narrower and show less relativistic effects, as emission from the inner surface, where the gravitational field is the strongest and the flow is the faster, is obscured. (3) Emission from semi-transparent accretion tori show more relativistic beaming effects. Processes forbidden in opaque disks/tori, such as resonance of lines with different wavelengths, can occur in semi-transparent disks, due to gravitational potential gradient and velocity shear. (4) Opaque scattering tori and opaque absorptive tori have different radiative properties, and an opaque scattering torus may not have a differential, weighted and relativistic energy-shifted thermal spectrum.

References

Baschek B., Efimov G.V., von Waldenfels W., Wehrse R., 1997, A&A, 317, 630

Cunningham C.T., 1975, ApJ, 202, 788

Fabian A.C., Rees M.J., Stella L., White N.E., 1989, MNRAS, 238, 729

Fabian A.C., Iwasawa K., Reynolds C.S., Young A.J., 2000, PASP, 112, 1145

Fuerst S.V., 2005, PhD Thesis, University of London

Fuerst S.V., Wu K., 2004, A&A, 424, 733

Fuerst S.V., Wu K., 2007, A&A, submitted

Laor A., 1991, ApJ, 376, 90

Lee K.-G., Fuerst S.V., Branduardi-Raymont G., Wu K., Crowley O., 2007, PASA, submitted.

Lindquist R., 1996, Annals of Physics, 37, 487

Magdziarz P., Zdziarski A.A., 1995, MNRAS, 273, 387

Misner C.W., Thorne K.S., Wheeler J.A., 1973, Gravitation, San Francisco: W H Freeman

Mizuno Y., Nishikawa K.I., Koide S., Hardee P., Fishman G.J., 2006a, ApJS, submitted (astro-ph/0609004)

Mizuno Y., Nishikawa K.I., Koide S., Hardee P., Fishman G.J., 2006b, ApJ, submitted (astro-ph/0609344)

Nandra K., George I.M., Mushotzky R.F., Turner T.J., Yaqoob T., 1999, ApJ, 523, L17

Stella L., 1990, Nature, 344, 741

Tanaka Y. et al., 1995, Nature, 375, 659

Wu K., Fuerst S.V., Lee K.-G., Branduardi-Raymont G., 2006, Chin. J. Astron. Astrophys. (ChJAA), 6 (Suppl. 1), 205

This paper was prepared with the ChJAA LaTeX macro v1.0.